

Article

Effect of Gas Recycling on the Performance of a Moving Bed Temperature-Swing (MBTSA) Process for CO₂ Capture in a Coal Fired Power Plant Context

Giorgia Mondino, Carlos A. Grande and Richard Blom *

SINTEF Materials and Chemistry, P. O. Box 124 Blindern, 0314 Oslo, Norway;
giorgia.mondino@sintef.no (G.M.); carlos.grande@sintef.no (C.A.G.)

* Correspondence: Richard.blom@sintef.no; Tel.: +47-90622647

Academic Editor: Fernando Rubiera González

Received: 2 April 2017; Accepted: 20 May 2017; Published: 25 May 2017

Abstract: A mathematical model of a continuous moving-bed temperature-swing adsorption (MBTSA) process for post-combustion CO₂ capture in a coal-fired power plant context has been developed. Process simulations have been done using single component isotherms and measured gas diffusion parameters of an activated carbon adsorbent. While a simple process configuration with no gas re-circulation gives quite low capture rate and CO₂ purity, 86% and 65%, respectively, more advanced process configurations where some of the captured gas is recirculated to the incoming flue gas drastically increase both the capture rate and CO₂ purity, the best configuration reaching capture rate of 86% and CO₂ purity of 98%. Further improvements can be achieved by using adsorbents with higher CO₂/N₂ selectivity and/or higher temperature of the regeneration section.

Keywords: CO₂ capture; adsorbents; post-combustion; moving bed; temperature-swing; process modelling; gPROMS; gas recycling

1. Introduction

The use of solid adsorbents is an alternative approach that may alleviate many of the problems connected to the liquid absorption processes. On a solid adsorbent the adsorption sites are spatially separated on a carrier, thus avoiding possible chemical degradation through site interaction. The number of adsorption sites is in most cases dependent on the surface area of the carrier, and often a linear relationship exists between the adsorption capacity of an adsorbent and its specific surface area. In addition, a good solid adsorbent will be chemically and physically stable at the operating conditions giving negligible loss of volatiles and good recyclability.

For post-combustion CO₂ capture, both pressure/vacuum swing adsorption (PSA/VSA) and temperature swing adsorption (TSA) processes have been suggested. For post-combustion CO₂ capture in a natural gas fired power plant (NGCC) context, where the partial pressure of CO₂ is small (typically around 4 vol %), regeneration with temperature swing may be more appropriate [1,2], while for CO₂ concentrations above 10 vol % VSA processes can also be considered.

For conventional fixed bed TSA processes, two factors limit the process performance: a high pressure drop over the adsorbent bed and slow heating and cooling rates. The moving bed temperature swing adsorption (MBTSA) concept offers the possibility to overcome the pressure drop in the section removing CO₂ and also allow faster heating and cooling of the adsorbent. The MBTSA concept was first suggested by Clyde Berg in the late 40s [3]. Later, the process has been thoroughly described by Ruthven in his classic book on adsorption processes [4]. For CO₂ capture, the MBTSA process was suggested by Knaebel in 2005 in which hot flue gas was used to indirectly heat the adsorbent during regeneration [5], and recently, researchers at SRI International has reported results from the

development of MBTSA process development using direct heating with steam during regeneration with carbon-based adsorbents [6]. Also researchers from Kawasaki in Japan published results from a CO₂ capture test for moving-bed system, however, lacking information about the process details and adsorbent used [7]. Kim and coworkers showed by modelling how the energy demand of the process can be significantly reduced by heat exchange between the hot adsorbent leaving the desorber with the cold adsorbent entering the desorber [8,9]. We have recently shown that reduced energy penalty compared to state-of-art amine based capture can be achieved when using the MBTSA process in a post-combustion NGCC context [10].

In this communication, we present results from MBTSA process modelling using activated carbon as adsorbent in a post-combustion coal fired power plant context using a realistic flue gas composition. We also show how the use of partial recirculation of gas from the upper part of the desorber unit can be used to improve the performance of the MBTSA process leading to higher capture rates and improved CO₂ purity.

2. Materials and Methods

2.1. Moving Bed TSA for CO₂ Capture

Differently from a conventional TSA process, where the adsorbent is packed in columns alternating between feed and regeneration mode, in a moving bed process the adsorbent is moving through different sections, each of which having a specific function. The three main sections composing the process in a MBTSA process are the adsorption (feed) section, the desorption (regeneration) section and the cooling section (see schematic drawing in Figure 1). From the top of the unit, the fresh adsorbent enters the adsorption section and moves downwards counter-currently to the feed gas stream, which is fed at the bottom of the section. The CO₂ contained in the flue gas is selectively removed by the sorbent, so that a CO₂-depleted gas is produced at the top of the unit. At the same time, the adsorbent leaving the feed section at the bottom is saturated with CO₂. In order to ensure a uniform distribution of the solid flow inside the column a structured packing may be used.

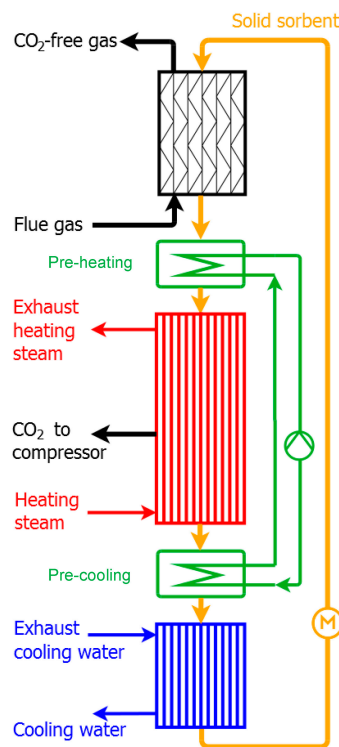


Figure 1. Schematic diagram of the MBTSA system.

Part of the heat required for sorbent regeneration is delivered in a pre-heating section. This step is important for heat integration: heat from the hot adsorbent powder leaving the regeneration section will be transferred to the cold adsorbent powder entering the regeneration section. Both these sections are operated as indirect contact heat exchangers, similarly to the desorption and the cooling sections. In the pre-cooling section, the adsorbent leaving the regeneration section exchanges heat with a fluid used to preheat the adsorbent in the pre-heating section, so that the net heat duty of the system is reduced. The target for process performance was to achieve a capture rate of at least 85% and a purity of the CO₂ product stream of at least 95%.

2.2. Process Modelling

The mathematical model used to describe the MBTSA process consists in a set of partial differential equations (unsteady and one dimensional) obtained by applying the mass, energy and momentum balance to the individual sections (adsorption, desorption and cooling section). In order to simulate the MBTSA process, the detailed mathematical model with appropriate boundary conditions was implemented in gPROMS modelling environment (PSE Enterprise, London, UK). More details about the model equations and the use of gPROMS as simulation tool for implementing the model can be found in Appendix A. The simulations were performed by discretizing the axial space domain of each process sections with the Centered Finite Difference Method (CFDM), with second order approximation. The number of intervals employed to discretize the axial space domain was 600 for the adsorption and the cooling sections, and 100 for the preheating and the desorption sections.

2.3. Simulation Conditions

2.3.1. Flue Gas Conditions

The flue gas conditions in terms of flowrate, temperature, pressure and composition were taken from a reference 800 MWe coal-fired power plant. Simulations were carried out by neglecting the presence of SO₂ in the flue gas, and assuming the same behaviour for Ar and O₂ as for N₂. It was then possible to consider a 3-component mixture rather than a 6-component mixture, and thus significantly simplify the problem in terms of computational effort. Based on the gas specifications provided in Table 1, and conserving the total number of moles, the flue gas flowrate and molar fractions were calculated and used in the moving bed TSA simulations.

Table 1. Flue gas specifications used in the MBTSA simulations.

Parameter (unit)	Value
Temperature (°C)	47
Pressure (bar)	1.05
Mass flowrate (kg/s)	198.6
Density (kg/m ³)	1.159
Composition (vol %):	
Inerts (N ₂ + O ₂ + Ar)	76.243
CO ₂	13.597
H ₂ O	10.160

2.3.2. Adsorbent Material

The activated carbon beads used was delivered by MAST Carbon International Ltd. (Basingstoke, UK). The characterization of this adsorbent in terms of adsorption isotherms of the main flue gas components, surface area, particles size and heat capacity is reported in Table 2 and Figure 2. The measured adsorption isotherms, were fitted with the Virial model in order to obtain the parameters required by the moving bed TSA model. The Virial model was selected for being suitable to fit non-type one isotherms, such as water isotherms, and for presenting the extension for predicting the

multi-component adsorption, which allows accounting for the competitive adsorption of the various gases in the system. The details are described in Appendix B.

Table 2. Adsorbent properties.

Property (unit)	Value
Particles size (mm)	0.5
Particles density (kg/m ³)	800
Specific heat capacity (J/kg/K)	880
Surface area (m ² /g)	1314

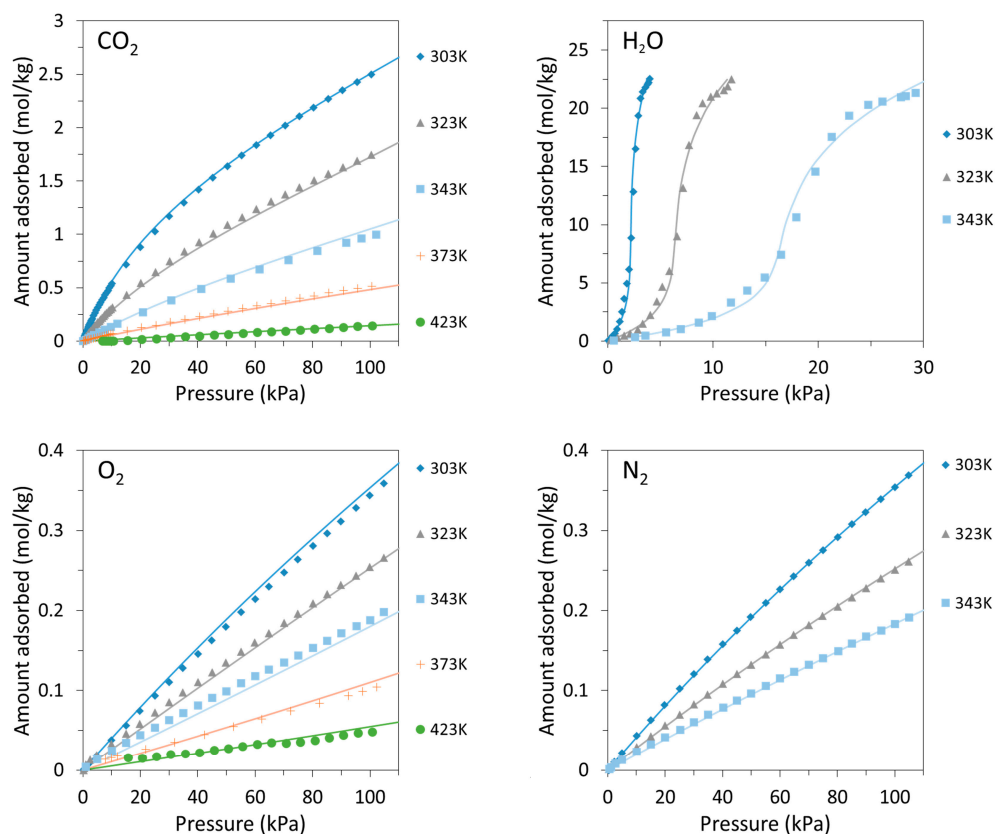


Figure 2. Adsorption isotherms of CO₂, H₂O, O₂ and N₂ on the activated carbon beads: experimental (dotted lines) and Virial isotherm fitting (solid lines).

3. Results

As previously mentioned the developed model was used to simulate a MBTSA process for capture of CO₂ from the reference coal-fired power plant. Due to the large amount of flue gas to be treated (almost 800 kg/s), it was decided to employ four MBTSA units in parallel. Given the feed gas conditions (temperature, pressure, flowrate), the column diameter was determined by considering a gas velocity in the adsorption section such that the particles cannot be fluidized.

Starting from a basic configuration, the MBTSA system was modified several times in order to investigate the effect of different operating modes with the objective of improving the process performance in terms of CO₂ purity and capture rate. The basic configuration and the proposed modifications that were implemented and successfully simulated will be described in the next paragraphs. Table 3 presents an overview of process configurations with their main characteristics, while Figure 3 shows the corresponding gPROMS simulations flowsheets.

Table 3. List of implemented configurations of the MBTSA system.

System Configuration ID	Extraction of Gas from Preheating Section	Recirculation of Extracted Gas into Feed Stream
Conf-A	No extraction	no
Conf-B	at the bottom (co-current gas-solid flow)	no
Conf-C	at the top (counter-current gas solid flow)	no
Conf-D	at the top (counter-current gas-solid flow)	yes

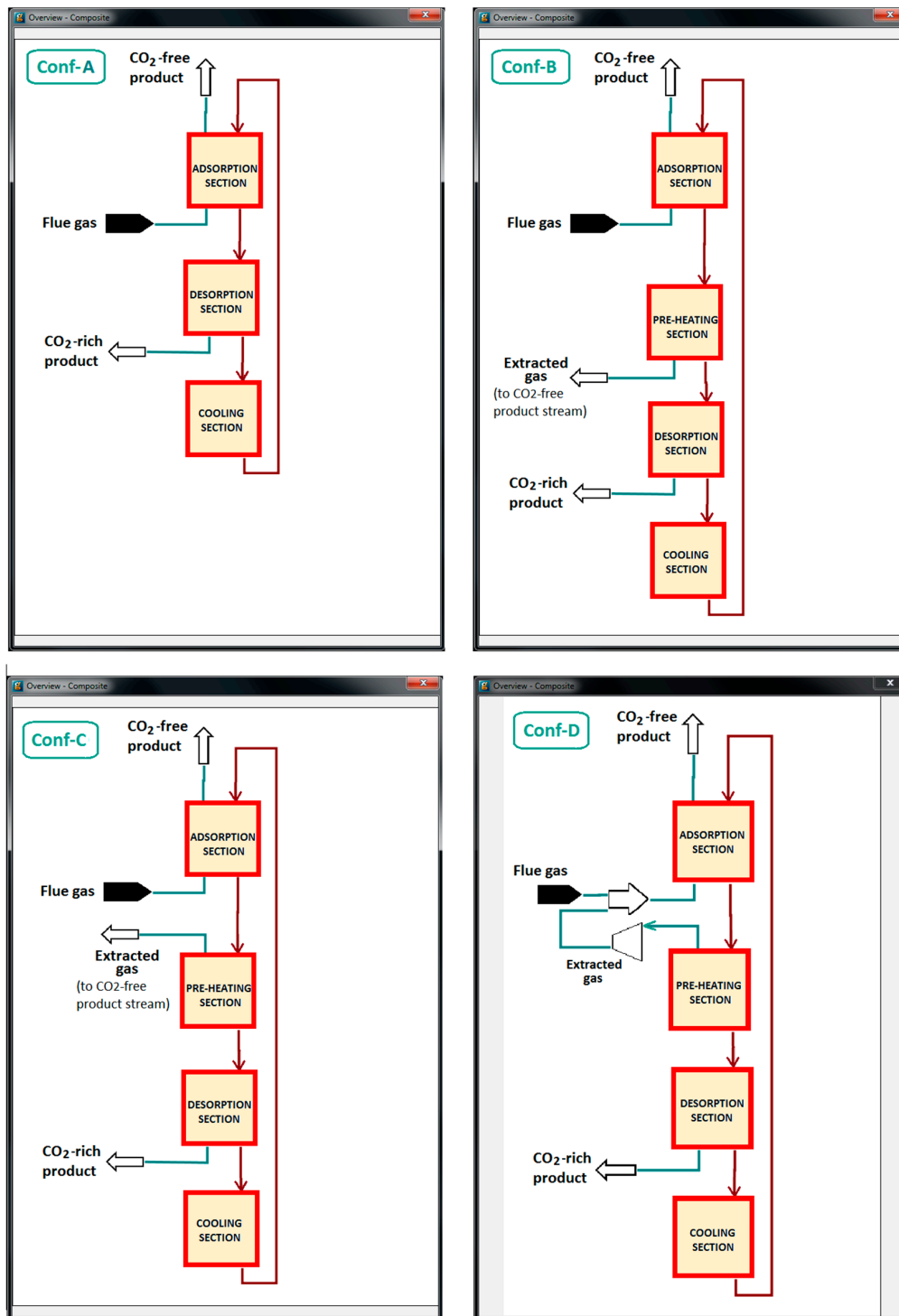


Figure 3. gPROMS flowsheets used for different configurations of the MBTSA system.

3.1. Basic Configuration (Conf-A)

As basic configuration of the MBTSA system, indicated here as Conf-A, the proposed system configuration is composed of three main parts: the adsorption section, the desorption section and the cooling section. The model of each section was implemented in gPROMS in a composite model, which allows to simultaneously simulate the whole MBTSA. The gPROMS flowsheet corresponding to the basic configuration is shown in Figure 3, where the red lines represents the solid sorbent streams and the green lines represent the feed gas stream, including the two products streams. Table 4 reports the main model parameters used in the simulations.

Table 4. Design parameters used in MBTSA simulations.

MBTSA Section	Parameter	Symbol	Unit	Value
Adsorption section	Column length	L_c	m	1.5
	Column radius	R_c	m	10
	Bed void fraction	ϵ_c		0.8
Pre-heating section	Column length	L_c	m	0–2
	Column radius	R_c	m	10
	Column void fraction	ϵ_c		0.6
	Outlet gas pressure	P_{out}	bar	0.99
Desorption section parameters	Column length	L_c	m	9
	Column radius	R_c	m	10
	Column void fraction	ϵ_c		0.6
	Outlet gas pressure	P_{out}	bar	0.96
Cooling section	Column length	L_c	m	12–15
	Column radius	R_c	m	10
	Column void fraction	ϵ_c		0.6

Under the studied conditions the simulated process was able to achieve the target of process performances in terms of capture rate (86.1%) but not in terms of CO₂ purity (65.0%). The reason for this was attributed to the relatively low selectivity of the adsorbent material towards CO₂, and the high concentration of N₂ in the flue gas of which a significant amount is also adsorbed together with the CO₂.

3.2. Introduction of Preheating Section with Co-Current Gas-Solid Flow (Extraction of Gas at the Bottom, Conf-B)

The first process modification implemented for the MBTSA consisted in introducing a preheating section in between the adsorption section and the desorption section, with the purpose of extracting part of the gas from the upper part of the desorption section, which contains mostly N₂. Initially, it was decided to operate the preheating section in a similar manner to the desorption section, in which the gas flows downwards (co-currently to the sorbent) and is withdrawn at the bottom of the column by applying a slight vacuum. As shown in Figure 3, in this first modified configuration (indicated here as Conf-B), the extracted gas is assumed to be returned to the power plant together with the CO₂-free product stream.

A series of simulations were performed for Conf-B, by varying the length of the pre-heating section in order to investigate the effect of such design parameter on the process performances. Some other design parameters, such as the length of the desorption and the cooling sections were also varied, compared to the Conf-A case, as reported in Table 5.

As reported in Table 5 and Figure 4, the results obtained by simulations of Conf-B show that the extraction of gas from the preheating section does have a positive effect on the CO₂ purity, which reaches 75.3% in the case with the longest preheating section. However, due to presence of CO₂ in the extracted gas, the obtained capture rate is lower compared to the previous configuration. Since the gas is extracted by applying slight vacuum at the outlet of the pre-heating section (bottom), the longest the section, the largest is the amount of gas extracted, and thus the lowest is the CO₂ recovery.

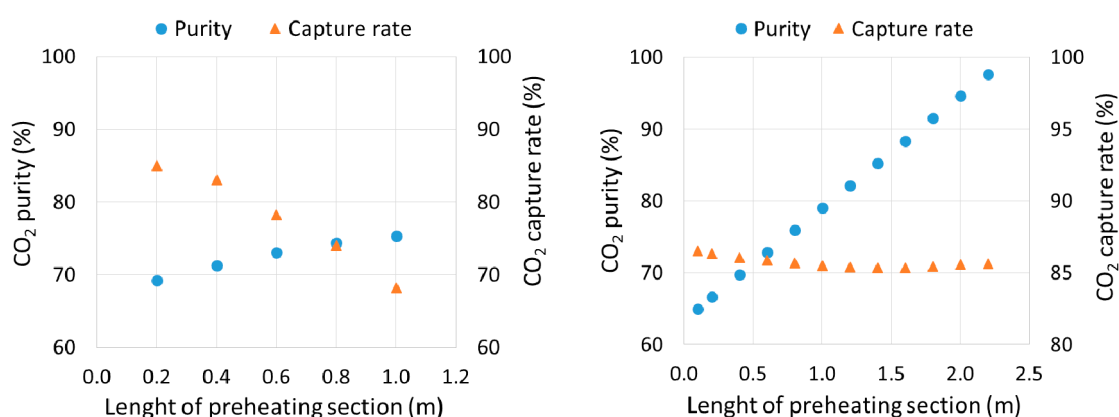


Figure 4. Effect of amount of length of preheating section on process performances for configuration B (left) and configuration D (right).

Table 5. Effect of length of preheating section on process performances for configuration B.

Simulation ID (unit)	B-1	B-2	B-3	B-4	B-5
Length of preheating section (m)	0.2	0.4	0.6	0.8	1.0
Length of cooling section (m)	12	14	14	14	14
Circulating amount of sorbent (kg/s)	2280	2280	2280	2280	2280
CO ₂ purity (%)	69.2	71.3	73.0	74.4	75.3
CO ₂ capture rate (%)	85.0	83.0	78.2	74.0	68.2

3.3. Preheating Section with Counter-Current Gas-Solid Flow/Extraction of Gas from Preheating Section From the Top (Conf-C)

For Conf-C the direction of the gas flow in the preheating section was inverted. By applying the slight vacuum at the top of the section rather than at the bottom, the gas flows upwards counter-currently to the solid sorbent. An improvement on both the CO₂ purity and CO₂ capture rate is expected as at the upper part of the preheating section corresponds the lowest content of CO₂.

As for Conf-B, the process was simulated for different lengths of the preheating section. The obtained results are summarized in Table 6 and Figure 4. As expected, extracting the gas from the top of the section rather than from the bottom has a beneficial effect on both the purity and the capture rate. For example, when using a 0.6 m long pre-heating section, a CO₂ purity of 75.2% with a 78.6% capture rate are obtained in the case of Conf-C, versus a 73.0% purity and 78.2% capture rate in the case of Conf-B.

Table 6. Effect of length of preheating section on process performances for Conf-C.

Simulation ID (unit)	C-1	C-2	C-3
Length of preheating section (m)	0.6	0.8	1.2
Length of cooling section (m)	14	15	15
Circulating amount of sorbent (kg/s)	2280	2280	2280
CO ₂ purity	75.2	77.9	83.9
CO ₂ capture rate	78.6	76.5	74.2

3.4. Recirculation of Extracted Gas into the Feed Gas Stream (Conf-D)

In order to avoid the loss of CO₂ associated to the extraction of gas from the preheating section, and thus improve the capture rate, it was decided to recirculate the extracted gas into the feed gas stream. Similar gas re-circulation steps have been used successfully in PSA processes in order to improve productivity and product stream purity [11].

The system was again simulated for different lengths of the pre-heating section, from 0.1 to 2.2 m, as shown in Table 7. In order to compensate for the higher feed gas flowrate, implied by the recirculation of extracted gas, it was necessary to increase the amount of circulating solid sorbent. The length of the cooling section was also increased, in order to assure that the adsorbent is cooled down to the same temperature as in the previous cases, and thus the same CO₂ cyclic capacity is maintained. The best results (Simulation D-15, with 97.6% purity and 85.6% capture rate) were obtained with a sorbent flowrate of 2550 kg/s which is approximately 12% higher than the previous cases. As previously mentioned, the length of the preheating section was found to be an important parameter for system designing, as it significantly affects the purity of the CO₂ product. The effect of such design parameters on the system behaviour can be seen in Figure 5, which shows a comparison of the gas compositions profiles in the preheating and desorption sections obtained for three different lengths of preheating section. As the molar fraction of N₂ decreases along the axis, from the solid inlet (top of the section) to the solid outlet (bottom of the section), the longer the preheating section, the lower is the N₂ content in the adsorbent entering the desorption section, and thus the higher is the CO₂ purity obtained in the desorption section. Figure 4 shows the results in term of CO₂ purity and CO₂ capture rate obtained for the set of simulations in which the same amount of circulating sorbent and the same length of cooling section was employed. While almost no effect on the CO₂ capture rate is observed, the CO₂ purity is linearly increased from 65% to nearly 98%. For the same set of simulations, Figure 6 shows the temperature of the solid, the adsorbed concentration of N₂ and the amount of gas extracted (expressed as ratio of extracted gas over flue gas flowrates) obtained at the solid outlet of the preheating section (bottom of the section). Obviously, for the longest preheating section, the highest temperature is reached by the adsorbent, and highest is the amount of N₂ desorbed and extracted from this section.

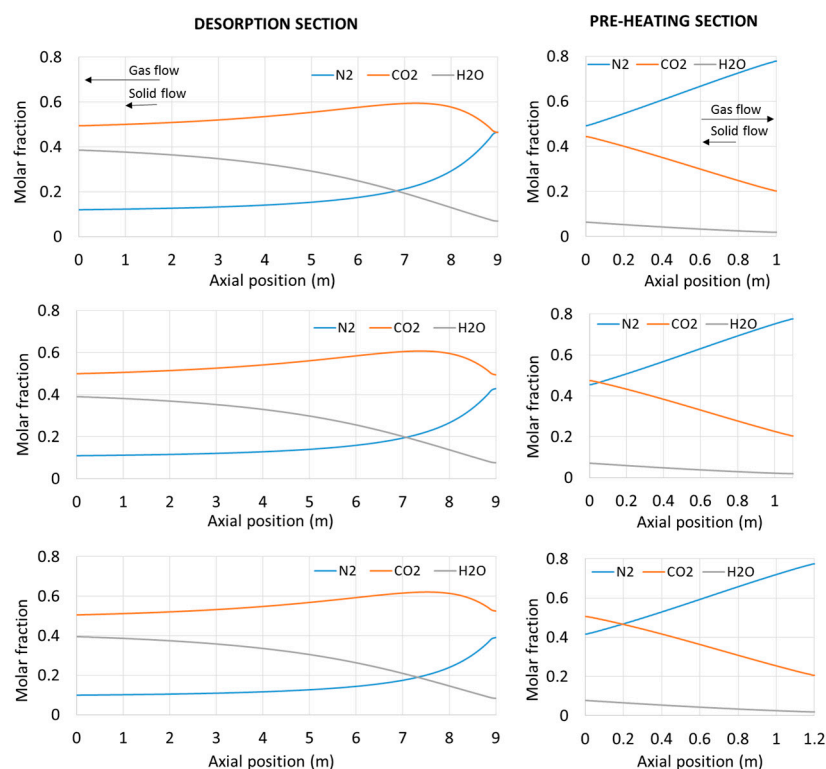


Figure 5. Gas composition profiles in desorption and preheating sections. Comparison of different lengths of the preheating section (1.0 (D-7) (top), 1.1 (D-8) (center), and 1.2 m (D-10) (bottom)).

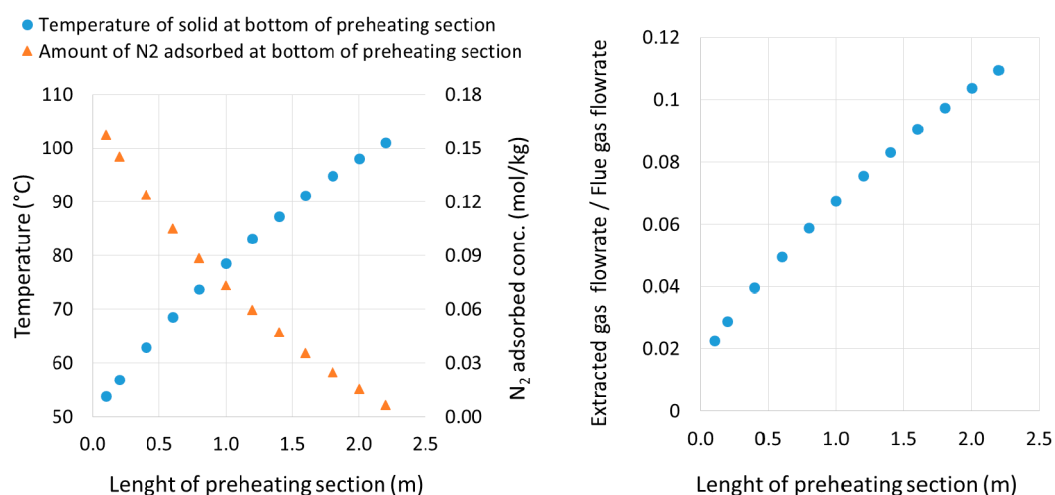


Figure 6. System configuration D: adsorbent temperature and N₂ adsorbed concentration at the outlet of preheating section (**left**) and amount of extracted gas (**right**) for different lengths of preheating section.

The behaviour of the full system can be observed in Figure 7, which shows the gas concentrations, adsorbed amounts and temperature profiles reached at steady state in each section of the MBTSA system. As expected, the adsorbed amount of CO₂ obtained at the bottom of the adsorption section (solid outlet) is close to the equilibrium capacity corresponding to the local sorbent-gas temperature and pressure conditions. However, due to the high concentration of N₂ in the flue gas, when the adsorbent leaves the adsorption section, also a significant amount of N₂ is adsorbed.

The temperature profiles along the adsorption section shows that the increase in temperature due to heat of adsorption is highest when H₂O adsorbs, since H₂O presents the highest heat of adsorption and the highest affinity to the adsorbent. After heating the adsorbent, first in the preheating section and then in desorption section, the cycle is closed in the cooling section, where the adsorbent is cooled down to the adsorption temperature. Simulations have shown that the system is very sensitive to this temperature, as the CO₂ capacity of the adsorbent is strongly dependent on the incoming adsorbent temperature. Higher inlet temperature means lower CO₂ capacity; the sorbent temperature at the outlet of the cooling section should be low enough to maintain the required CO₂ cyclic capacity.

4. Discussion

Table 8 summarizes the results from the MBTSA simulations. In the basic MBTSA process configuration, Conf-A, the adsorbent flows from the adsorption section into a desorption section where the adsorbent is heated leading to regeneration of the adsorbent. After a cooling step, the adsorbent, still carrying a certain amount of CO₂ is re-entered at the top of the adsorption section for a new cycle. The activated carbon adsorbent has a CO₂/N₂ selectivity of around 12 at the flue gas composition. With such a low selectivity also significant amount of nitrogen will be adsorbed at the exit of the adsorption section. In addition the pores will be filled with flue gas, so at the entrance of the regeneration section, when starting to heat the adsorbent powder, nitrogen will first be released, before desorption of carbon dioxide. This leads to a quite good capture rate (86.1%, but with a low CO₂ purity (65.0%).

Table 7. Effect of length of preheating section on process performances for configuration D.

Simulation ID	D-1	D-2	D-3	D-4	D-5	D-6	D-7	D-8	D-9	D-10	D-11	D-12	D-13	D-14	D-15
Length of preheating section (m)	0.1	0.2	0.4	0.6	0.6	0.8	1	1.1	1.2	1.2	1.4	1.6	1.8	2	2.2
Length of cooling section (m)	15	15	15	15	14	15	15	15	15	15	15	15	15	15	15
Circulating amount of sorbent (kg/s)	2550	2550	2550	2550	2400	2550	2550	2450	2550	2500	2550	2550	2550	2550	2550
Extracted gas flow/flue gas flow (%)	2.3	2.9	4.0	5.0	4.9	5.9	6.8	7.0	7.6	7.5	8.3	9.0	9.7	10.4	11.0
Temperature of adsorbent at the bottom of preheating section (°C)	53.8	56.9	62.9	68.5	70.4	73.7	78.6	82.6	83.1	84.0	87.3	91.2	94.8	98.1	101.0
Amount of N ₂ adsorbed at the bottom of preheating section (mol/kg)	0.16	0.14	0.12	0.11	0.09	0.09	0.07	0.06	0.06	0.06	0.05	0.04	0.02	0.02	0.01
CO ₂ purity (%)	65.0	66.7	69.8	72.9	76.0	76.0	79.1	81.7	82.2	82.6	85.3	88.4	91.5	94.6	97.6
CO ₂ capture rate (%)	86.5	86.3	86.1	85.8	87.1	85.6	85.5	81.9	85.4	83.4	85.3	85.3	85.4	85.6	85.6

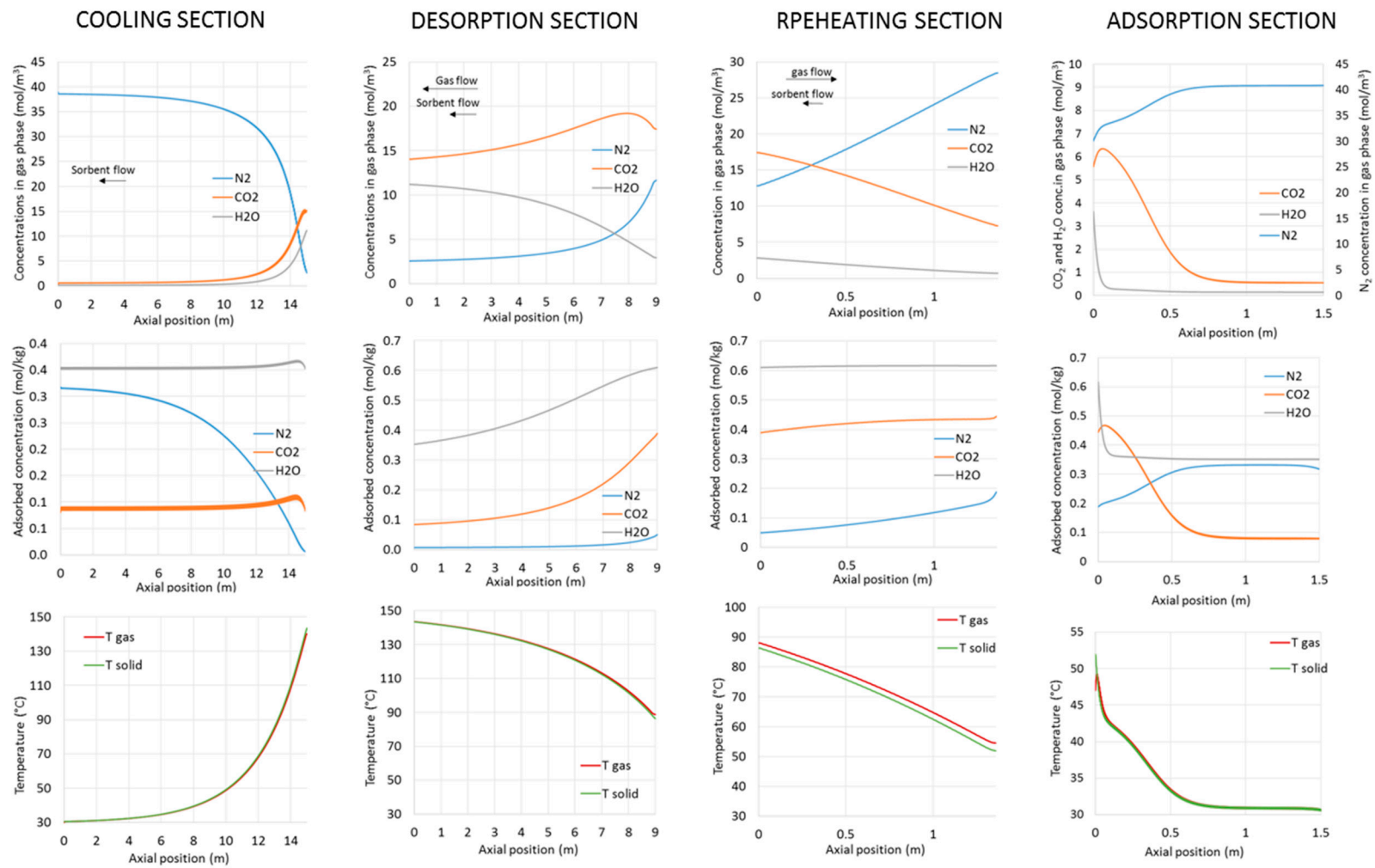


Figure 7. Gas concentration (**top row**), adsorbent loading (**middle row**), and temperature profiles (**bottom row**) along the MBTSA sections. From left to right: cooling section, desorption section, preheating section and adsorption section (Data from simulation case D-11).

Table 8. Summary of results from different MBTSA process configurations.

Simulation ID	Length of Preheating Section (m)	System Configuration	CO ₂ Purity (%)	CO ₂ Capture Rate (%)
Sim-A1	0	Conf-A (basic)	65.0	86.1
Sim-B3	0.6	Conf-B (extraction from the bottom)	73.0	78.2
Sim-C1	0.6	Conf-C (extraction from the top)	75.2	78.6
Sim-D4	0.6	Conf-D (extraction from the top, with recirc.)	72.9	85.8
Sim-D15	2.2	Conf-D (extraction from the top, with recirc.)	97.6	85.6

In Conf-B and Conf-C a pre-heating section has been inserted between the adsorption section and the regeneration section. However, the gas extracted, either at the bottom (Conf-B) or at the top (Conf-C) of the pre-heating section is only removed and emitted together with the exit gas from the adsorber. The extracted gas is rich in nitrogen but still contains significant amounts of carbon dioxide. Consequently, the extraction improves somewhat the CO₂ purity of the CO₂ rich product stream, but at the same time, it lowers the overall capture rate since more CO₂ is lost to the exit gas from the adsorption section.

For Conf-D, the gas extracted from the top of the pre-heating section is recycled to the incoming flue gas. By doing this, the steady-state concentration of CO₂ in the feed gas entering the adsorbent section slightly increases (For D-15 from 13.6% to 14.3%) since the recycled gas that in volume is about 10% of the flue gas, contains 21.2% CO₂. For this configuration, the capture rate increases back to similar value as for Conf-A, namely 85.6%. We find that the CO₂ purity of the product stream is strongly dependent on the length of the pre-heating section: Increasing the length of this section from 0.6 to 2.2 m leads to an increase in the CO₂ product purity from 73% to 98%, the last value being well above the target set by the European Best Practice Guidelines for Assessment of CO₂ Capture Technologies [12].

Initial simulations using the same adsorption equilibrium data for CO₂ as used in the simulations presented above, but mimicking higher CO₂/N₂ selectivity by lowering the nitrogen isotherm, show that significant improvement in the MBTSA performance will be achieved with an adsorbent having higher selectivity. In addition, preliminary results show that improved performance will also be achieved when using higher regeneration temperature, however, this certainly also will lead to higher energy consumption. Further improvement of the MBTSA process together with work on alternative, more advanced adsorbents to be used for the MBTSA process is ongoing.

5. Conclusions

Based on mathematical modelling of a MBTSA process using an activated carbon material as adsorbent in a post-combustion coal fired power plant context, we find that CO₂ capture rates higher than 85% and CO₂ product stream purities higher than 97% is only achievable if some of the gas desorbed during the initial phase of the regeneration process (in the pre-heating section) are extracted and re-circulated to the incoming flue gas. The reason why re-circulation is necessary is a consequence of both high porosity of the adsorbent material, causing a relatively large amount of flue gas following inside the pores of the adsorbent, and partly because of a relatively low CO₂/N₂ selectivity of activated carbon at the relevant gas composition leading to a relatively high fraction of adsorbed nitrogen.

The activated carbon adsorbent seems to work satisfactory also in the presence of water vapour when regeneration takes place at 150 °C and above. Keeping the regeneration temperature as low as possible is necessary to keep the energy penalty of the process at a low level.

The main challenge when using an activated carbon as adsorbent is the relatively low working capacity achieved, resulting in the need of four MBTSA processes in parallel to treat all the flue gas from an 800 MW_e coal-fired power plant. Significant reduction in the footprint would be achieved with an adsorbent having higher working capacity. Also, an adsorbent having a higher CO₂/N₂ selectivity would reduce the volume of necessary re-cycling and thus contribute to the reduction in process size.

Acknowledgments: We acknowledge financial support from the Norwegian Research Council and Statoil (grant no. 221137), from the EU FP7 project HiPerCap (grant no. 608555) and from the Polish-Norwegian Research Program through the SolSorb project (grant no. 237761).

Author Contributions: G.M. built up a gPROMS model under supervision by C.A.G., G.M. also carried out the MBTSA simulations in discussions with R.B., G.M., C.A.G. and R.B. have written the manuscript together.

Conflicts of Interest: The authors declare no conflict of interest.

Nomenclature

A_c	Bed cross sectional area (m ²)
A	First Virial coefficient
a'	Particle specific area (m ² /kg)
B	Second Virial coefficient
Bi_i	Biot number of component i
c_p	Gas mixture molar specific heat at constant pressure (J/mol/K)
c_v	Gas mixture molar specific heat at constant volume (J/mol/K)
$c_{v,i}$	Molar specific heat at constant volume for component i (J/mol/K)
C	Third Virial coefficient
$C_{b,i}$	Molar concentration of component i in the macropores (mol/m ³)
C_i	Molar concentration of component i (mol/m ³)
C_T	Total gas concentration (mol/m ³)
D_c	Micropore diffusivity (m ² /s)
d_{we}	Wall external diameter (m)
d_{wi}	Wall internal diameter (m)
D_m	Molecular diffusivity (m ² /s)
D_p	Macropore diffusivity of (m ² /s)
D_z	Axial dispersion coefficient (m ² /s)
e	Wall thickness (m)
K_{eq}	Equilibrium constant of component i
K_{eq}^∞	Equilibrium constant at infinite temperature
h_f	film heat transfer coefficient between the gas and the particle (J/s/m ² /K)
h_w	film heat transfer coefficient between the gas and the wall (J/s/m ² /K)
k_m	Film mass transfer coefficient
L_c	Column length (m)
P	Pressure (Pa)
P_i	Initial pressure
P_{atm}	Atmospheric pressure
Pe_i	Peclet number of component i
Q_{feed}	Volumetric flowrate of feed gas (m ³ /s)
q_i	Adsorbed phase concentration of component i (mol/kg)
q_i^*	Adsorbed concentration of component i in equilibrium with $C_{b,i}$ (mol/kg)
R	Ideal gas constant (J/K/mol)
R_b	Bed radius (m)
r_p	Particle radius (m)
T_{feed}	Temperature of the feed gas
T	Temperature of the gas
T_s	Temperature of the solid
u	Superficial velocity of the gas (m/s)
v_{solid}	Velocity of the solid (m/s)
$Y_{feed,i}$	Molar fraction of component i in the feed gas
Y_i	Molar fraction of component i
ΔH	Isosteric heat of adsorption (kJ/mol)
U	Global heat transfer coefficient (m/s)

Greek Symbols

α_w	ratio of the internal surface area to the volume of the column wall (m ⁻¹)
α_{wl}	ratio of the logarithmic surface area of the column shell to the volume of the column wall (m ⁻¹)
ϵ_c	Bed porosity
ϵ_p	Particle porosity
ζ	Packing porosity factor
ρ_{gas}	Gas density (kg/m ³)
ρ_{pack}	Packing density (kg/m ³)
ρ_p	Particle density (kg/m ³)
λ	Heat axial dispersion coefficient (J/m/s/K)

Appendix A

In order to simulate the TSA moving bed process, a detailed mathematical model was developed and implemented in gPROMS modelling environment (PSE Enterprise, London, UK). The model consists of a set of unsteady one-dimensional partial differential equations including mass, energy and momentum balances. The same set of coupled differential equations, distributed over the vertical axial domain, is applied to each

section (adsorption, desorption, preheating and cooling section) and has to be solved simultaneously during simulations. For this purpose the individual section-models were connected to each other in a so-called gPROMS Composite model. With the composite model approach, the different sections communicate with each other through an appropriately defined “variables-port”. The purpose of the model ports is to transfer certain variables at the boundaries of the corresponding space domain, so that the model instances can exchange information with the other model instances during simulation. For the MBTSA composite model, two different port types were defined: a “solid port”, for exchanging variables corresponding to the adsorbent (adsorbed phase concentration, temperature of the solid, etc.) and a “gas port” for exchanging information on the gas phase (gas concentration, gas composition, temperature, etc.). As an example, as boundary conditions for the solid phase at the top of the adsorption section (solid inlet), the variables computed within the cooling section at the bottom of the process (solid outlet) are assigned. In this way, the conditions of the solid leaving the cooling section are used as input conditions at the top of the adsorption section (solid inlet). This allows for example to take into account for a non-perfect regeneration of the solid sorbent performed in the desorption section, which in turn will affect the performance of the adsorption section.

By assuming that mass, velocity and temperature gradients in the radial direction are negligible, one-dimensional macroscopic balance equations on the axial coordinate are considered. The model also assumes constant cross sectional area, constant solid velocity and constant void fraction along the column.

More specifically the moving bed adsorption system comprises a gas phase, which exchanges energy and mass with the solid sorbent and only energy with the wall, a solid phase onto which the gas diffuses and adsorbs, and the column wall through which heat can be transferred from (or to) the surroundings.

For the gas phase, the mass balance in a differential element of the column of coordinate z for component i is expressed as:

$$\varepsilon_c \frac{\partial C_i}{\partial t} = \varepsilon_c \frac{\partial}{\partial z} \left(D_z C_T \frac{\partial Y_i}{\partial z} \right) - \frac{\partial(uC_i)}{\partial z} - \frac{(1 - \varepsilon_c - \xi)a'K_{m,i}}{Bi/5 + 1} (C_i - C_{b,i}) \quad (A1)$$

To describe the mass transfer rate in the solid phase the linear driving force model (LDF) is employed. The resulting equation of mass balance in the solid phase is given by:

$$\varepsilon_p \frac{\partial C_{b,i}}{\partial t} = \varepsilon_p \frac{15D_{p,i}}{r_p^2} \frac{Bi_i}{5 + Bi_i} (C_i - C_{b,i}) - \rho_p \left(\frac{\partial q_i}{\partial t} + v_{solid} \frac{\partial q_i}{\partial z} \right) - v_{solid} \frac{\partial C_{b,i}}{\partial z} \quad (A2)$$

where is $C_{b,i}$ and q_i are the particle averaged concentration of component i in the macro-pores and adsorbed, respectively. Two important terms of the previous equations that distinguish the model from a fixed-bed adsorption model are $v_{solid} \frac{\partial q_i}{\partial z}$ and $v_{solid} \frac{\partial C_{b,i}}{\partial z}$ which represent the contributions due to the movement of the solid along the axial coordinate, v_{solid} being the velocity of the solid. The same term $v_{solid} \frac{\partial q_i}{\partial z}$ appears in the LDF equation for the micro-pore of the adsorbent (solid diffusion equation):

$$\frac{\partial q_i}{\partial t} + v_{solid} \frac{\partial q_i}{\partial z} = \frac{15D_{c,i}}{r_c^2} (q_i^* - q_i) \quad (A3)$$

In this equation q_i^* is the adsorbed concentration of component i in equilibrium with the concentration of the same component in the gas phase inside the pore $C_{b,i}$.

The adsorption equilibrium of the gases onto the solid is described by the Virial adsorption model, which presents the following extension of single component equilibrium to predict multi component systems [13–16]:

$$C_{b,i}RT = \frac{q_i^*}{Keq_i} \exp \left[\sum_{j=1}^N A_{ij}q_j^* + \sum_{j=1}^N \sum_{k=1}^N B_{ijk}q_j^*q_k^* + \sum_{j=1}^N \sum_{k=1}^N \sum_{l=1}^N C_{ijkl}q_j^*q_k^*q_l^* \right] \quad (A4)$$

$$Keq_i = K_{eq,i}^\infty \exp \left(\frac{-\Delta H_i}{RT_s} \right) \quad (A5)$$

$$A_i = A_{0,i} + \frac{A_{1,i}}{T_s} B_i = B_{0,i} + \frac{B_{1,i}}{T_s} C_i = C_{0,i} + \frac{C_{1,i}}{T_s} \quad (A6)$$

$$A_{ij} = \frac{A_i + A_j}{2} B_{ijk} = \frac{B_i + B_j + B_k}{3} C_{ijkl} = \frac{C_i + C_j + C_k + C_l}{4} \quad (A7)$$

Due to the high void fraction in the bed, the Ergun equation is not employed in the momentum balance, which is instead given by:

$$-\frac{\partial P}{\partial z} = (\rho_p - \rho_{gas})a_E \cdot u \quad (A8)$$

where a_E is assumed to be 0.2 s^{-1} .

As mentioned previously the energy balance is divided in three different equations: one for the gas phase, one for the solid phase and one for the column wall.

For the gas phase the energy balance is given by:

$$\varepsilon_c C_T c_v \frac{\partial T}{\partial t} = \frac{\partial}{\partial z} \left(\lambda \frac{\partial T}{\partial z} \right) - u C_T c_p \frac{\partial T}{\partial z} - (1 - \varepsilon_c - \xi) a' h_f (T - T_s) - \frac{2h_w}{R_b} (T - T_w) \quad (\text{A9})$$

In this equation, the term $(1 - \varepsilon_c - \xi) a' h_f (T - T_s)$ represents the energy exchanged by the gas phase with the solid, h_f being the convective heat transfer coefficient between the gas phase and the solid particles. In the same equation, the term $\frac{2h_w}{R_b} (T - T_w)$ represents the thermal energy exchanged between the gas and the column wall, h_w being the convective heat transfer coefficient between the gas and the wall, T_w the wall temperature and R_b the radius of the column.

Similar terms appear in the energy balance in the solid phase, which is given by:

$$\begin{aligned} & \left[(1 - \varepsilon_c - \xi) \rho_p c_{ps} + \xi \rho_{pack} c_{ppack} \right] \left(\frac{\partial T_s}{\partial t} + v_{solid} \frac{\partial T_s}{\partial z} \right) \\ & = \xi \frac{\partial}{\partial z} \left(\lambda_{pack} \frac{\partial T_s}{\partial z} \right) + (1 - \varepsilon_c - \xi) a' h_f (T - T_s) + (1 - \varepsilon_c \\ & - \xi) \rho_p \sum \left(-\Delta H_i \left[\frac{\partial q_i}{\partial t} + v_{solid} \frac{\partial q_i}{\partial z} \right] \right) + (1 - \varepsilon_c \\ & - \xi) \varepsilon_p R T_s \sum \left[\frac{\partial C_{b,i}}{\partial t} + v_{solid} \frac{\partial C_{b,i}}{\partial z} \right] \end{aligned} \quad (\text{A10})$$

Finally, the energy balance across the column wall is given by:

$$\rho_w c_{p,w} \frac{\partial T_w}{\partial t} = \alpha_w h_w (T - T_w) - \alpha_{w1} U (T_w - T_\infty) \quad (\text{A11})$$

where T_w and T_∞ are the wall and the external temperatures, respectively, U is the overall heat transfer coefficient between the external surface of the column and the surroundings and α_w and α_{w1} are defined by:

$$\alpha_w = d_{wi} / [e(d_{wi} + e)] \quad (\text{A12})$$

$$\alpha_{w1} = 1 / [(d_{wi} + e) \ln((d_{wi} + e) / d_{wi})] \quad (\text{A13})$$

where e is the wall thickness.

The following correlations were used to calculate heat and mass transport parameters appearing in the model. For the pore diffusivity a combination of molecular and Knudsen diffusivity is assumed [4]:

$$\frac{1}{D_p} = \tau_p \left(\frac{1}{D_k} + \frac{1}{D_m} \right) \quad (\text{A14})$$

where D_k is the Knudsen diffusivity obtained as:

$$D_k = 97 r_p \sqrt{\frac{T}{M_w}} \quad (\text{A15})$$

and D_m is the molecular diffusivity calculated using the Wilke correlation [17]:

$$D_m = \frac{1 - y_i}{\sum_{j \neq i}^n \frac{y_j}{D_{ij}}} \quad (\text{A16})$$

where D_{ij} is the binary molecular diffusivity calculated with the Chapman-Enskog equation [18]:

$$D_{ij} = \frac{2.66 \times 10^{-2} T^{3/2}}{P M_{ij}^{1/2} \sigma_{ij}^2 \Omega_{D_{ij}}} \quad (\text{A17})$$

In order to estimate the heat and mass axial dispersion coefficients the following empirical correlations can be employed [4,19,20]:

$$D_z = \frac{D_m}{\varepsilon_c} (20 + 0.5 Sc Re) \quad (\text{A18})$$

$$\lambda = k_g (7 + 0.5 Pr Re) \quad (\text{A19})$$

$$Nu = 2.0 + 1.1 Re^{0.6} Pr^{1/3} \quad (\text{A20})$$

$$Sh = 2.0 + 1.1Re^{0.6} Sc^{1/3} \quad (A21)$$

The dimensionless numbers appearing in the previous correlations are defined as follow:

$$Re = \frac{\rho_g u_0 D_p}{\mu_g}; Sc = \frac{\mu_g}{\rho_g D_m}; Pr = \frac{C_{p,g} \mu_g}{k_g}; Sh = \frac{k_f d_p}{D_m}; Nu = \frac{h_f d_p}{k_g} \quad (A22)$$

In order to study the performance of the MBTSA process under investigation, the CO₂ purity and capture rate were calculated as follow:

$$\text{Purity}_{\text{CO}_2} (\text{dry}) = \frac{y_{\text{CO}_2}}{1 - y_{\text{H}_2\text{O}}} \Big|_{\text{in the CO}_2 \text{ product stream}} \quad (A23)$$

$$\text{Capture rate}_{\text{CO}_2} = \frac{\dot{M} y_{\text{CO}_2} \frac{1000}{\sum_i (y_i M_{w,i})} \Big|_{\text{in the CO}_2 \text{ product stream}}}{\dot{M} y_{\text{CO}_2} \frac{1000}{\sum_i (y_i M_{w,i})} \Big|_{\text{in the flue gas}}} \quad (A24)$$

where \dot{M} is the mass flowrate (in kg/s), $M_{w,i}$ is the molecular weight of component i (in g/mol), y_i is the molar fraction of component and n is the number of components. Unlike in a conventional temperature or pressure swing adsorption, where the definition of performance parameters includes an integral term in order to account for the variations over time in flowrate and products composition [21,22], here the integral term is not required as CO₂ purity and capture rate are evaluated once the system has reached steady state. The above equations apply to all system configurations described in the main text.

Appendix B

Adsorption isotherms were measured for the main flue gas components (N₂, CO₂, H₂O and O₂) using a commercial adsorption apparatus (Belsorp-Max, MicrotracBEL). The measurements were performed at temperatures between 30 and 150 °C up to atmospheric pressure, with the exception of the water isotherms, which were measured up their corresponding saturation pressure. Prior to the measurements, the sample was degassed at 120 °C under vacuum overnight.

Measurements of diffusion parameters for the main flue gas components have also been performed, by means of pulse chromatography method (for N₂, CO₂ and O₂) and breakthrough curves (for H₂O), showing rapid adsorption kinetics. Details on the experimental method and apparatus used for this purpose can be found elsewhere [23].

The experimental adsorption equilibrium data were fitted with the Virial model, which is given by [14,24]:

$$P = \frac{q}{K} \exp(Aq + Bq^2 + Cq^3) \quad (A25)$$

where P is the gas pressure, q is the amount adsorbed, K is the Henry constant, and A , B and C are the Virial coefficients. The Henry constant is related to the temperature through the Van't Hoff equation:

$$K = K_\infty \exp\left(-\frac{\Delta H^0}{R_g T}\right) \quad (A26)$$

where K_∞ is the adsorption constant at infinite temperature, T is the temperature, ΔH^0 is the heat of adsorption at zero coverage and R_g is the universal gas constant. The temperature dependence of the Virial coefficients described by:

$$A = A_0 + \frac{A_1}{T}, B = B_0 + \frac{B_1}{T}, C = C_0 + \frac{C_1}{T} \quad (A27)$$

Fitting of the pure component adsorption data was carried out using Scilab (<http://www.scilab.org>) defining an error function as:

$$ERR (\%) = 100 \sum_T \sum_i \left(\frac{q_{cal} - q_{exp}}{q_{cal}} \right)^2 \quad (A28)$$

where T is each experimental temperature, i is the number of point of each isotherm, q_{cal} is the calculated amount adsorbed and q_{exp} is the experimental amount adsorbed. The error was minimized with the Nelder-Mead algorithm by applying the *fminsearch* optimization algorithm provided by Scilab. The fitting parameters are reported in Table A1 and were employed in the prediction of multicomponent adsorption equilibrium using the extension of the Virial model [20], as described in Appendix A.

Table A1. Fitting parameters of the Virial model for N₂, CO₂, O₂, H₂O on the carbon beads.

Gas	K_{∞}	$-\Delta H^0$	$A_0 \times 10^2$	A_1	$B_0 \times 10^2$	B_1	$C_0 \times 10^5$	C_1
	mol/kg/kPa	kJ/mol	kg/mol	kg/mol	(kg/mol) ²	(kg/mol) ²	(kg/mol) ³	(kg/mol) ³
N ₂	6.334×10^{-6}	16.371	-33.145	244.701	0	0	0	0
CO ₂	6.963×10^{-8}	35.162	-27.271	288.978	-87.660	239.320	0	0
O ₂	2.849×10^{-6}	18.317	-432.19	1433.73	0	0	0	0
H ₂ O	2.355×10^{-8}	44.242	-37.616	49.560	2.718	-6.323	-58.411	0.171

References

- Humphrey, J.L.; Keller, G.E. *Separation Process Technology*; McGraw-Hill: New York, NY, USA, 1997.
- Wankat, P.C. *Separation Process Engineering*, 2nd ed.; Prentice Hall: Upper Saddle River, NJ, USA, 2006.
- Berg, C. Hypersorption process for separation of light gases. *Trans. AIChE* **1946**, *XLII*, 665–680.
- Ruthven, D.M. *Principles of Adsorption and Adsorption Processes*; John Wiley & Sons: New York, NY, USA, 1984; p. 391.
- Knaebel, K.S. Temperature Swing Adsorption System. U.S. Patent 7594956 B2, 29 September 2009.
- Hornbostel, M.D.; Bao, J.; Krishnan, G.; Nagar, A.; Jayaweera, I.; Kobayashi, T.; Sanjurjo, A.; Sweeney, J.; Carruthers, D.; Petruska, M.A.; et al. Characteristics of an advanced carbon sorbent for CO₂ capture. *Carbon* **2013**, *56*, 77–85. [[CrossRef](#)]
- Okumura, T.; Ogino, T.; Nishibe, S.; Nonaka, Y.; Shoji, T.; Higashi, T. CO₂ capture test for a moving-bed system utilizing low-temperature steam. *Energy Procedia* **2014**, *63*, 2249–2254. [[CrossRef](#)]
- Kim, K.; Park, Y.-K.; Park, J.; Jung, E.; Seo, H.; Kim, H.; Lee, K.S. Performance comparison of moving and fluidized bed sorption systems for an energy-efficient solid sorbent-based carbon capture process. *Energy Procedia* **2014**, *63*, 1151–1161. [[CrossRef](#)]
- Kim, K.; Son, Y.; Lee, W.B.; Lee, K.S. Moving bed adsorption process with internal heat integration for carbon dioxide capture. *Int. J. Greenh. Gas Control* **2013**, *17*, 13–24. [[CrossRef](#)]
- Grande, C.A.; Kvamsdal, H.; Mondino, G.; Blom, R. Development of moving bed temperature swing adsorption (MBTSA) process for post-combustion CO₂ capture: Initial benchmarking in a NGCC context. *Energy Procedia* **2017**, in press.
- Santor, M.S.; Grande, C.A.; Rodrigues, A.E. New cycle configuration to enhance performance of kinetic PSA processes. *Chem. Eng. Sci.* **2011**, *66*, 1590–1599. [[CrossRef](#)]
- The European Benchmark Task Force. Available online: <http://www.co2cesar.eu/site/en/downloads.php> (accessed on May 2012).
- Taqvi, S.M.; LeVan, M.D. Virial description of two-component adsorption on homogeneous and heterogeneous surfaces. *Ind. Eng. Chem. Res.* **1997**, *36*, 2197–2206. [[CrossRef](#)]
- Ribeiro, A.M.; Sauer, T.P.; Grande, C.A.; Moreira, R.F.; Loureiro, J.M.; Rodrigues, A.E. Adsorption equilibrium and kinetics of water vapor on different adsorbents. *Ind. Eng. Chem. Res.* **2008**, *47*, 7019–7026. [[CrossRef](#)]
- Shen, C.; Liu, Z.; Li, P.; Yu, J. Two-stage VPSA process for CO₂ capture from flue gas using activated carbon beads. *Ind. Eng. Chem. Res.* **2012**, *51*, 5011–5021. [[CrossRef](#)]
- Ribeiro, A.M.; Grande, C.A.; Lopes, F.V.; Loureiro, J.M.; Rodrigues, A.E. Four beds pressure swing adsorption for hydrogen purification: Case of humid feed and activated carbon beds. *AIChE J.* **2009**, *55*, 2292–2302. [[CrossRef](#)]
- Wilke, C.R. Diffusional properties of multicomponent gases. *Chem. Eng. Prog.* **1950**, *46*, 95–104.
- Bird, R.B.; Stewart, W.E.; Lightfoot, E.N. *Transport Phenomena*, 2nd ed.; Wiley: New York, NY, USA, 2002.
- Wakao, N.; Funazkri, T. Effect of fluid dispersion coefficients on particle-to-fluid mass transfer coefficients in packed beds: Correlation of Sherwood numbers. *Chem. Eng. Sci.* **1978**, *33*, 1375–1384. [[CrossRef](#)]
- Yang, R.T. *Gas Separation by Adsorption Processes*; Butterworth-Heinemann: Boston, MA, USA, 2013.
- Grande, C.A. Advances in pressure swing adsorption for gas separation. *ISRN Chem. Eng.* **2012**, *2012*, 1–13. [[CrossRef](#)]
- Liu, Z.; Grande, C.A.; Li, P.; Yu, J.; Rodrigues, A.E. Multi-bed vacuum pressure swing adsorption for carbon dioxide capture from flue gas. *Sep. Purif. Technol.* **2011**, *81*, 307–317. [[CrossRef](#)]

23. Masala, A.; Vitillo, J.G.; Mondino, G.; Grande, C.A.; Blom, R.; Manzoli, M.; Marshall, M.; Bordiga, S. CO₂ capture in dry and wet conditions in UTSA-16 metal organic framework. *ACS Appl. Mater. Interfaces* **2016**, *9*, 455–463. [[CrossRef](#)] [[PubMed](#)]
24. Shen, C.; Grande, C.A.; Li, P.; Yu, J.; Rodrigues, A.E. Adsorption equilibria and kinetics of CO₂ and N₂ on activated carbon beads. *Chem. Eng. J.* **2010**, *160*, 398–407. [[CrossRef](#)]



© 2017 by the authors. Licensee MDPI, Basel, Switzerland. This article is an open access article distributed under the terms and conditions of the Creative Commons Attribution (CC BY) license (<http://creativecommons.org/licenses/by/4.0/>).